of dark noise in the *Limulus* retina. At night, efferent nerve signals from a circadian clock in the brain reduce the rate of spontaneous events from photoreceptors and second-order cells without affecting those evoked by light[15,16]. The Arrhenius energies for noise generation are nearly equal both day and night (Fig. 2), indicating that the clock does not reduce noise by increasing the energy required to generate it.

We propose that dark noise in *Limulus* photoreceptors results from the thermal isomerization of a small (<0.01%) population[17] of rhodopsin molecules containing unprotonated Schiff-base chromophores. At night the clock's efferent input reduces noise by decreasing the number of molecules in the unprotonated state and does so by lowering external pH in the vicinity of the rhodopsin-containing membrane.

Figure 3 presents tests of this molecular mechanism. Mimicking the clock's efferent input by delivering current shocks to the optic nerve decreases retinal pH by 0.14 units (Fig. 3*a*). Mimicking the efferent input as in Fig. 3*a* reduces retinal dark noise as measured by spontaneous optic nerve activity (Fig. 3*b*). The reduction of noise follows by ~1 min the transient decrease in pH. Why the noise changes outlast the the pH changes is not clear. Injecting the eye with mildly acidic saline (pH 6.86) reduces photoreceptor dark noise ~50 times, which corresponds well with the observations in *Limulus* ventral photoreceptors of noise reduction by low pH[18] and the accessibility of visual pigment to changes in extracellular pH[19] (Fig. 3*c*). Neural activity lowers pH in other tissues[20]. Efferent inputs to the *Limulus* eye terminate directly on rhodopsin-containing membranes of each photoreceptor[21], but how they can lower pH is not known. The source may be presynaptic activity because agonists of the efferent input that act postsynaptically do not strongly influence photoreceptor noise[22,23]. In summary, the results of these physiological tests are consistent with the molecular mechanism we propose.

Horseshoe crabs have evolved circadian mechanisms for increasing the sensitivity of their lateral eyes at night, apparently to help them find mates at the water's edge[24,25]. With a relatively high content of rhodopsin[21], *Limulus* photoreceptors are highly sensitive but noisy. The theoretical and experimental studies we report here support the idea that the circadian efferent input to the photoreceptors reduces their noise by reducing the small population of relatively unstable, unprotonated rhodopsin molecules.

Whether other animals modulate photoreceptor dark noise as we propose for *Limulus* is not known. The near proportionality between dark noise and rhodopsin content of photoreceptors in a variety of animals[1,10,26,27] points to rhodopsin as the noise source. Some animals such as insects[27] and primates[26] may minimize dark noise by possessing relatively small photoreceptors with correspondingly small amounts of rhodopsin. Animals such as toads and other amphibians with large photoreceptors and large amounts of rhodopsin per cell may minimize dark noise by living at relatively low temperatures[4]. Finally, the pH of some vertebrate photoreceptors decreases under prolonged dark adaptation[28,29], leaving open the possibility that rhodopsin stabilization contributes to high visual sensitivity in these animals as it appears to in *Limulus*. □

Received 15 June; accepted 24 August 1993.

1. Baylor, D. A., Matthews, G. & Yau, K. W. *J. Physiol.* **309,** 591–621 (1980).
2. Yeandle, S. *Am. J. Ophthalmol.* **46,** 82–87 (1958).
3. Copenhagen, D. R., Donner, K. & Reuter, T. J. *J. Physiol.* **393,** 667–680 (1987).
4. Aho, A. C., Donner, K., Hyden, C., Larsen, L. O. & Reuter, T. *Nature* **334,** 348–350 (1988).
5. Barlow, H. B. *J. Opt. Soc. Am.* **46,** 634–639 (1956).
6. Barlow, H. B. *Nature* **334,** 296–297 (1988).
7. Birge, R. R. *Biochim. biophys. Acta* **1016,** 293–327 (1990).
8. Tallent, J. R., Hyde, E. W., Findsen, L. A., Fox, G. C. & Birge, R. R. *J. Am. chem. Soc.* **114,** 1581–1592 (1992).
9. Schick, G. A., Cooper, T. M., Holloway, R. A., Murray, L. P. & Birge, R. R. *Biochemistry* **26,** 2556–2562 (1987).
10. Ashmore, J. F. & Falk, G. *J. Physiol.* **332,** 272–297 (1977).
11. Hubbard, R. *J. biol. Chem.* **241,** 1814–1818 (1966).
12. Longstaff, C., Calhoon, R. D. & Rando, R. R. *Proc. natn. Acad. Sci. U.S.A.* **83,** 4209–4213 (1986).
13. Sakmar, T. P., Franke, R. R. & Khorana, H. G. *Proc. natn. Acad. Sci. U.S.A.* **86,** 8309–8313 (1989).
14. Fahmy, K. & Sakmar, T. P. *Biochemistry* **32,** 9165–9171 (1993).
15. Barlow, R. B. Jr, Kaplan, E., Renninger, G. H. & Saito, T. *J. gen. Physiol.* **89,** 353–378 (1987).
16. Kaplan, E. & Barlow, R. B. Jr *Nature* **286,** 393 395 (1980).
17. Birge, R. R. *Biophys. J.* **64,** 1371 1372 (1993).
18. Corson, D. W. & Fein, A. *Brain Res.* **193,** 558–561 (1980).
19. Lisman, J. E. & Strong, L. A. *J. gen. Physiol.* **73,** 219 243 (1980).
20. Chesler, M. *Prog. Neurobiol.* **34,** 401 427 (1990).
21. Fahrenbach, W. H. *Z. zeliforsch. mikrosk. anat.* **93,** 451–483 (1969).
22. Schneider, M. H., Lehman, H. K. & Barlow, R. B. Jr, *Invest. Ophth. Vis. Sci.* **28,** (suppl.) 186 (1987).
23. Kass, L., Pelletier, J. L., Renninger, G. H. & Barlow, R. B. Jr *J. comp. Physiol.* A**164,** 95–105 (1988).
24. Barlow, R. B. Jr, Ireland, L. C. & Kass, L. *Nature* **296,** 65–66 (1982).
25. Powers, M. K., Barlow, R. B. Jr & Kass, L. *Visual Neurosci.* **7,** 179 189 (1991).
26. Baylor, D. A., Nunn, B. J. & Schnapf, J. L. *J. Physiol.* **357,** 575–607 (1984).
27. Lillywhite, P. G. *J. comp. Physiol.* **122,** 189–200 (1977).
28. Borgula, G. A., Karwoski, C. J. & Steinberg, R. H. *Vision Res.* **29,** 1069–1077 (1989).
29. Oakley, B. II & Wen, R. *J. Physiol.* **419,** 353–378 (1989).
30. Smith, W. C., Greenberg, R. M., Price, D. A. & Battelle, B. A. *Invest. Ophth. Vis. Sci.* **33,** (suppl.) 1004 (1992).
31. Chesler, M. & Kraig, R. P. *Am. J. Physiol.* **253,** R666–R670 (1987).
32. Barlow, R. B. Jr *J. Neurosci.* **3,** 856 870 (1983).

ACKNOWLEDGEMENTS. We thank D. A. Baylor, P. A. Hargrave and T. P. Sakmar for discussions, and M. Chesler and T. H. Silbaugh for assistance. This research was supported by the National Science Foundation, the National Institutes of General Medical Science and the National Eye Institute.

Fast axonal transport is required for growth cone advance

Chris Martenson, Kimberly Stone, Mary Reedy & Michael Sheetz*

Departments of Pathology and Cell Biology, Duke University Medical Center, Durham, North Carolina 27710, USA

GROWTH cones are capable of advancing despite linkage to a stationary axonal cytoskeleton in chick and murine dorsal root ganglion neurites[1,2]. Several lines of evidence point to the growth cone as the site of cytoskeletal elongation[3,4]. Fast axonal transport is probably the means by which cytoskeletal elements[5] or cofactors are rapidly moved through the axon. We report that direct, but reversible, inhibition of fast axonal transport with laser optical tweezers inhibits growth cone motility if cytoskeletal attachment to the cell body is maintained. Advancement ceases after a distance-dependent lag period which correlates with the rate of fast axonal transport. But severing the axonal cytoskeleton with the laser tweezers allows growth cones to advance considerably further. We suggest that axon elongation requires fast axonal transport but growth cone motility does not.

In previous studies, when fast axonal transport was ligated by mechanical axonal transection, growth cones collapsed but then re-extended before halting[6,7]. Using optical tweezers capable of inhibiting the movement of intracellular vesicles non-invasively[8], we determined how growth cones respond when deprived of fast transport vesicles while remaining cytoskeletally linked to the cell body. Failure to advance under these conditions would suggest that factors carried by the fast transport system to the vicinity of the growth cone mediate the process of cytoskeletal elongation.

Directing the optical tweezers at a large vesicle, such as a mitochondria or a 1–2 μm intra-axonal varicosity, causes complete occlusion to vesicular transport in 1–2 min (Fig. 1). Initially, only large vesicles are halted by the tweezers but, as they accumulate, progressively smaller vesicles become trapped by the block. The result is an axonal swelling at the focal point of the optical tweezers. The rate at which the swellings induced by optical tweezers increased in diameter, and the final diameter

* To whom correspondence should be addressed.

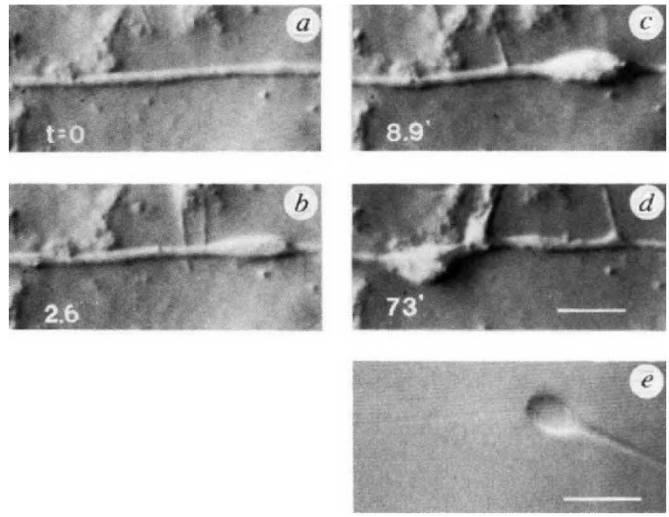

FIG. 1 Axonal blockage induced by laser tweezers, and subsequent recovery. *a*, Axon is 1.1 μm in diameter. Laser irradiation was for 5.6 min at 200 mW. No observable vesicular traffic traversed the block after 1.8 min of laser irradiation. Anterograde traffic proceeds from left to right. *b*, Same axon after 2.6 min. Growth of the bulge correlates with the influx volume of vesicles. *c*, Axon after 8.9 min. Vesicles accumulate for another 39 s, at which point they approach and traverse the blockage. *d*, Same axon after 73 min. The swelling has decreased in diameter and moved 18 μm retrogradely. Scale bar, 5 μm. *e*, View of laser-transected axon 5 min after 1.2 min of 200-mW laser irradiation. The diameter of axon seen to the right of the axoplasm 'bead' is comparable to the original diameter of the axon. Vesicle movements can be observed to the right of the 'bead', indicating membrane integrity. This bead of axoplasm withdrew towards the growth cone which is 124 μm to the right. The membranous tether is estimated to be 40–80 nm in diameter. Scale bar, 5 μm.

METHODS. Dorsal root ganglion explants were dissected from 12-day chick embryos and plated on poly-D-lysine-coated size 0 coverslips which had been exposed for 15 min to a 1:50 Matrigel:MEME solution. MEME without phenol red (GIBCO) was used as a base stock with 600 mg% (w/v) glucose, 20 mM HEPES buffer, 2 mM glutamine, 50 units per ml of penicillin and streptomycin, N2 supplement (GIBCO), and 75 mg ml^{-1} NGF. All experiments were illuminated by a mercury-arc halogen lamp passed through an ultraviolet, an infrared, and a 610-nm high-pass filter element. Three growth cones were tracked for 45 min each under this illumination and showed no observable defects in either morphology or rate of advance. Details of this laser-tweezers microscope system have been described[14].

of the swellings, correlated with the volume of axonal vesicular traffic. Electron micrographs of swellings induced by laser tweezers reveal an abundance of membranous profiles and continuous cytoskeletal elements throughout the block (Fig. 2). Vesicles neither stopped nor accumulated after defocusing the optical tweezers into a poor trapping configuration, indicating that the swellings are generated by the interaction between optical tweezers and vesicle and not by the dose of photons delivered.

Blocking vesicular transport within an axon stopped growth cone advance in all 29 growth cones investigated. Growth cones >190 μm from the block continued to advance during the blocking procedure and stopped abruptly after a lag period (Fig. 3*a*). The length of this lag period was linearly dependent on the distance between the block and the growth cone, with an average signalling rate of 1.28 μm s^{-1} (Fig. 3*d*). For ~70% of growth cones cessation of advance correlated with morphological alterations, characterized by a collapse of the lamellar regions and an increase in the length and number of filopodia.

The tweezers-induced blocks are not the result of irreversible damage because resumption of vesicular traffic across the block

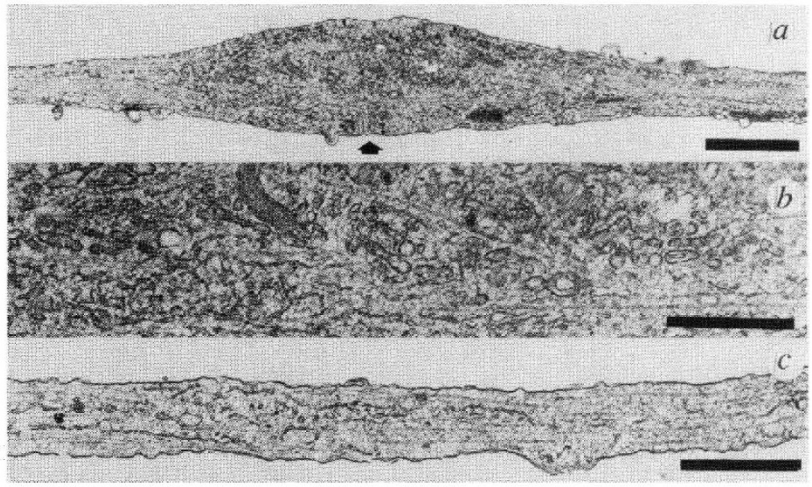

FIG. 2 Electron micrograph of laser-blocked axon. *a*, Axon was blocked for 1.5 min at 200 mW, with the centre of the beam focused at the location indicated by the arrowhead. Cell body is located to the left. The preponderance of trapped membrane is represented by endoplasmic reticulum-like tubulovesicular profiles. Similar profiles are seen in the axon on both sides of the block and in control axon sections. Integrity of axonal membrane, internal membranous features, and abundance of mitochondrial profiles indicate the axonal membrane remained intact throughout the procedure. Two other laser blocks, fixed with glutaraldehyde/tannic acid/osmium and embedded in araldite, also revealed accumulation of similar organelles. Scale bar, 2 μm. *b*, Higher magnification view of centre of same block. As in endogenous swellings on non-blocked axons, the microtubules and neurofilaments that traverse the block region are often distorted from a parallel orientation, probably being forced aside by the densely packed vesicles. Scale bar, 1 μm. *c*, Section of control axon reveals comparable membranous organelle profiles and preservation of axonal membrane. Scale bar, 1 μm.

METHODS. All laser irradiation and cell culture protocols are described in legend to Fig. 1, except that coverslips were first carbon-coated over electron microscope finder grids and ultraviolet light-sterilized. Immediately following block formation, the sample on the heated stage was fixed by flowing ~300–400 μl of 3% glutaraldehyde freshly diluted into the growth medium, pH 7.4. Post-fixation was in 1% OsO_4 in 0.2 M collidine buffer at 4 °C for 30 min. Sample was block-stained in 2% aqueous uranyl acetate for 30 min, dehydrated, and embedded in Epon. 70-nm longitudinal sections were collected in series and post-stained with uranyl acetate and lead citrate. Micrographs were photographed on a Phillips CM-10 transmission microscope.

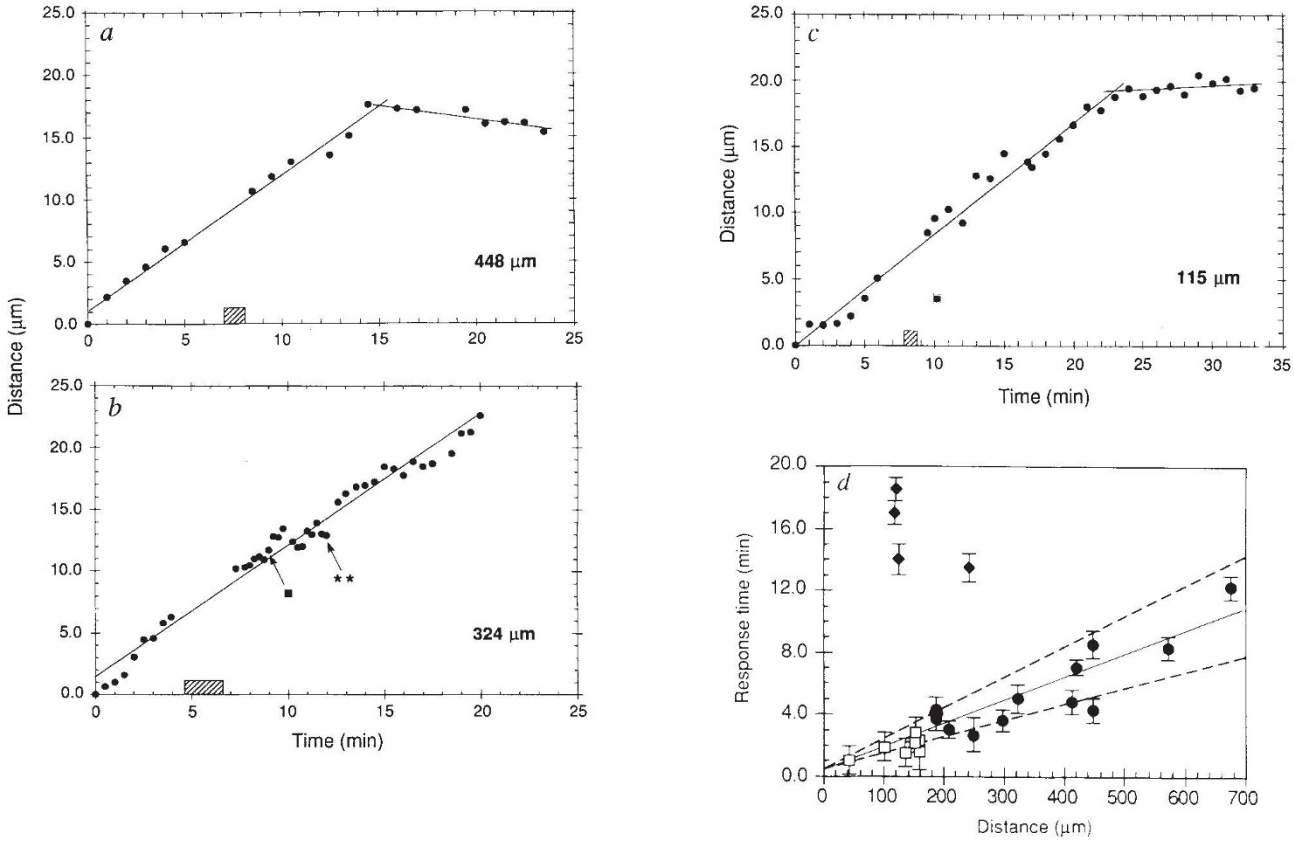

FIG. 3 *a*, Growth cone centroids measured before and after axon blockage. Laser irradiation 448 μm from the growth cone lasted 61 s at 200 mW (hatched rectangle on the ordinate). Growth cone advances for 8.5 min after the start of the optical-tweezing procedure indicating a signalling rate of 0.88 μm s^{-1}. Collapse of lamellar structures and cessation of growth cone advance occur at the point where the two slopes intersect at which a slow retraction commences. *b*, Growth cone centroids measured before and after blockage of the axon 324 μm away. Laser irradiation was for 1.9 min at 200 mW (hatched rectangle) and ceased the moment blockage was complete. The growth cone advances for 5.5 min from the start of lasering, indicating a signalling rate of 0.98 μm s^{-1}, loses most of its lamellar area (solid square), and ceases to advance for 2.25 min. Double asterisk indicates the resumption of advance, which in this case coincides with the sudden return of active lamellae. The forward weight provided by the lamellae accounts for the apparent forward jump of the growth cone. The post-recovery advance rate of 0.8 μm min^{-1}, although less than that of the pre-laser irradiation period, is comparable to the measured rate of most other control growth cones. *c*, Growth cone centroids after laser transection of the axon. Hatched rectangle on the ordinate indicates the period of laser irradiation at 200 mW and 115 μm from the growth cone. A rapid bidirectional retreat of axonal contents at the block site occurred after 1.0 min of irradiation. Growth cone continues to advance for 16.2 min after the start of laser irradiation. A non-transected growth cone would have ceased moving in 3 min. *d*, Growth-cone advance after laser irradiation for non-severed (filled circles), and transected (filled triangles) growth cones. Open squares represent growth cones that did not significantly advance. The slope of the best-fit line (solid line) through the non-severed data points indicates a signalling rate of 1.28 μm s^{-1}, with a 99% confidence interval of the slope (dotted lines), bounded by rates of 1.49 μm s^{-1} and 0.82 μm s^{-1}. A diffusion-driven response would operate as the square of the distance. Thus, a generated toxin diffusing through medium at 1×10^{-6} cm^2 s^{-1} would require at least 15 min to travel 300 μm and at least 81 min to travel 700 μm. Additionally, a diffusing toxin would be diluted by the cube of the distance. A toxin diffusing in the plane of a membrane at 1×10^{-8} cm^2 s^{-1} would require 10 times longer to travel equivalent distances. Error bars for all filled data points indicate the length of the lasering procedure. Error bars for the open squares indicate the length of time from the mid-point of the lasering procedure to the re-imaging of the growth cone.

METHODS. All experiments were recorded on a VHS videotape. Stored images were then digitized by a Scion 8-bit video board and stored as PICT files by IMAGE 1.47 (NIH) software. Each growth cone image was outlined and the *x* and *y* centroids calculated by Signal Analytic's IP-LABS program. All structures of the growth cone were included in the outline. The neck of the growth-cone was arbitrarily set to exist at the point where the axon swelled to 1.5 times its original diameter. No weighting was given to regions of varying optical (or biological) density.

sites occurred routinely after 1–3 min of laser irradiation. Additionally, recovery of normal growth cone motility and morphology was possible if the optical tweezers was turned off when a complete block had formed (Fig. 3*b*). To determine the effects of radiation damage, the optical tweezers were used intermittently (for a cumulative 3 min of laser irradiation) so that no vesicles became trapped and no axonal blockage formed. In these cases, no alterations in growth cone morphology or motility were noted. In addition, focusing the laser ⩽2 μm to the side of an axon for 3 min had no effect, ruling out local heating as a factor. However, recovery of normal growth cone morphology and motility did not correlate directly with the resumption of vesicle transport across the block site, indicating that some form of damage had occurred. Using longer exposures to laser light (3–5 min), a form of damage to membrane integrity was occasionally observed. In these cases, the growth cones collapsed and withdrew faster than they could be relocated and brought back in focus.

Cytoskeletal breaks, visualized as a rapid bidirectional withdrawal of axoplasm from the block region, sometimes occurred if laser irradiation was conducted within 250 μm of the growth cone. The severed axonal stumps usually remained 'linked' by an extremely thin membranous tether which was fluid and showed no vesicle movements, overt stiffness, or other indications of possessing a cytoskeletal structure (Fig. 1*e*). Severed growth cones continued to advance for at least 10–15 min longer

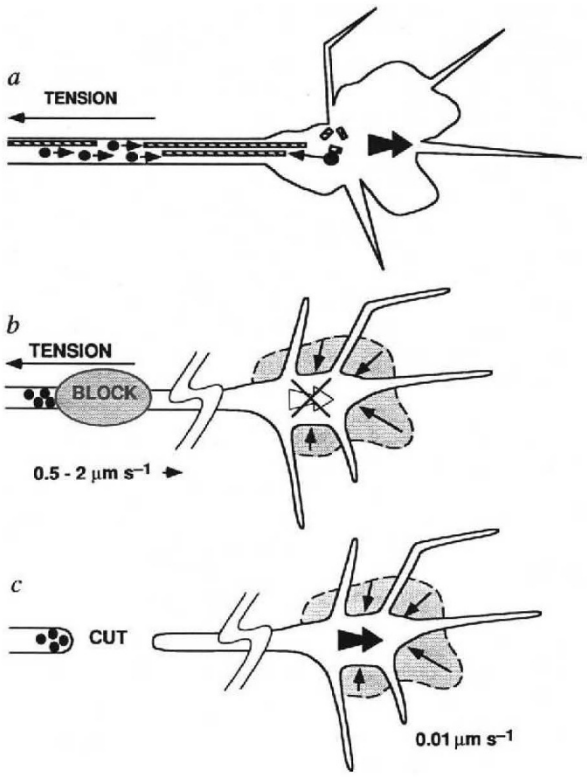

FIG. 4 Summary of growth cone behaviour. *a*, Factors carried by the fast transport system (filled circles) arrive at the growth cone and facilitate the elongation of the cytoskeletal network (hatched rectangles), allowing advance (solid arrow) to occur. *b*, When growth cones are deprived of fast transport material but remain attached to the axonal cytoskeleton, advance is no longer possible (crossed-out arrow) and growth cones collapse. These changes are propagated to the growth cone at the indicated rate of 0.5–2 $\mu m\ s^{-1}$. *c*, When growth cones are transected from the axonal cytoskeletal network and deprived of fast transport material, they collapse but are capable of advancing at the rate indicated. Thus, the only limitation to the forward movement of blocked growth cones is anchorage to the cytoskeleton.

than similarly irradiated non-severed growth cones (Fig. 3*c*). As both blocked and transected growth cones are deprived of fast transport vesicles to the same extent and have received equivalent doses of laser irradiation, cytoskeletal linkage to the cell body may account for the variance in motile behaviour. The possibility of a slow wave of Ca^{2+} influx propagating down the axon was ruled out as such waves in other systems are much more rapid[9]. Similarly, changes propagated as a result of a blockage of the slow transport system might be expected to travel at the slow transport rate of 0.01–0.05 $\mu m\ s^{-1}$.

The simplest explanation for our findings is that the axonal cytoskeleton provides a mechanical anchor to forward migration (Fig. 4*b*). For the axonal cytoskeleton to elongate in the absence of a bulk sliding process[1,2], cytoskeletal assembly must occur near the growth cone. Fast axonal transport of cytoskeletal elements may occur[5] but it is also likely that cytoskeletal proteins are conveyed by slow axonal transport (reviewed in ref. 10) and assembly is locally regulated at the growth cone. Such assembly could require fast transport components that either coassemble with the cytoskeleton or are short-lived cofactors in the assembly process (Fig. 4*a*). Transection (Fig. 4*c*) would relieve the tension axons are under[11–13], allowing the growth cone to advance. □

Received 11 May; accepted 7 September 1993.

1. Okabe, S. & Hirokawa, N. *J. Cell Biol.* **107,** 651–664 (1988)
2. Okabe, S. & Hirokawa, N. *Nature* **343,** 479–482 (1990).
3. Bamburg, J., Bray, D. & Chapman K. *Nature* **321,** 788–790 (1986).
4. Brown, A., Slaughter, T. & Black, M. *J. Cell. Biol.* **4,** 867–882 (1992).
5. Hollenbeck, P. & Bray, D. *J. Cell Biol.* **105,** 2827–2835 (1987).
6. Shaw, G. & Bray, D. *Exp. Cell Res.* **104,** 55–62 (1977).
7. Bray, D. *J. Cell Sci.* **37,** 391–410 (1979).
8. Ashkin, A., Schutze, K., Dziedzic, J., Euteneuer, U. & Schliwa, M. *Nature* **348,** 346–348 (1990).
9. Cornell-Bell, A., Finkbeiner, S., Cooper, M. & Smith, S. *Science* **247,** 470–473 (1990).
10. Mitchison, T. & Kirschner, M. *Neuron* **1,** 761–772 (1988).
11. Dennerll, T., Joshi, H., Steel, V., Buxbaum, R. E. & Heidemann, S. R. *J. Cell Biol.* **107,** 665–674 (1988).
12. Dennerll, T. J., Lamoureux, P., Buxbaum, R. & Heidemann, S. R. *J. Cell Biol.* **109,** 3073–3083 (1989).
13. Lamoureux, P., Buxbaum, R. E. & Heidemann, S. R. *Nature* **340,** 159–162 (1989).
14. Kucik, D., Kuo, S., Elson, E. & Sheetz, M. *J. Cell Biol.* **114,** 1029–1036 (1991).

ACKNOWLEDGMENTS. We thank. S. C. Kuo for technical assistance and for discussion.

Spontaneous loss of T-cell tolerance to glutamic acid decarboxylase in murine insulin-dependent diabetes

Daniel L. Kaufman*†‡, Michael Clare-Salzler §‖, Jide Tian*, Thomas Forsthuber‖¶, Grace S. P. Ting*, Paul Robinson§, Mark A. Atkinson#, Eli E. Sercarz¶, Allan J. Tobin†‡ & Paul V. Lehmann‖¶**

* Department of Psychiatry and Biobehavioral Sciences, § Department of Medicine, ¶ Department of Microbiology and Molecular Genetics, ** Department of Biology, † Brain Research Institute, and ‡ Molecular Biology Institute, University of California at Los Angeles, Los Angeles, California 90024, USA
# Department of Pathology and Laboratory Medicine, College of Medicine, University of Florida, Gainesville, Florida 32610, USA

INSULIN-DEPENDENT diabetes mellitus (IDDM) in non-obese diabetic (NOD) mice results from the T-lymphocyte-mediated destruction of the insulin-producing pancreatic β-cells and serves as a model for human IDDM[1]. Whereas a number of autoantibodies are associated with IDDM[2], it is unclear when and to what β-cell antigens pathogenic T cells become activated during the disease process. We report here that a T-helper-1 (Th1) response to glutamate decarboxylase develops in NOD mice at the same time as the onset of insulitis. This response is initially limited to a confined region of glutamate decarboxylase, but later spreads intramolecularly to additional determinants. Subsequently, T-cell reactivity arises to other β-cell antigens, consistent with intermolecular diversification of the response. Prevention of the spontaneous anti-glutamate decarboxylase response, by tolerization of glutamate decarboxylase-reactive T cells, blocks the development of T-cell autoimmunity to other β-cell antigens, as well as insulitis and diabetes. Our data suggest that (1) glutamate decarboxylase is a key target antigen in the induction of murine IDDM; (2) autoimmunity to glutamate decarboxylase triggers T-cell responses to other β-cell antigens, and (3) spontaneous autoimmune disease can be prevented by tolerization to the initiating target antigen.

We tested NOD mice from birth to 28 weeks of age for T-cell reactivity to β-cell antigens that are targets of IDDM-associated

‖ Present addresses: Department of Pathology and Laboratory Medicine, College of Medicine, University of Florida, Gainesville, Florida 32610, USA (M.C.-S.); and Department of Pathology, School of Medicine, Case Western Reserve University, Cleveland, Ohio 44106, USA (T.F. and P.V.L.).